Heliyon 8 (2022) e12644

Contents lists available at ScienceDirect

Heliyon

journal homepage: www.cell.com/heliyon

Research article

$ZnO/Cu_2O/g\text{-}C_3N_4$ heterojunctions with enhanced photocatalytic activity for removal of hazardous antibiotics

Yujie Zhu [a], Ling Wang [b], Wentao Xu [c], Zehai Xu [a,*], Junsheng Yuan [c], Guoliang Zhang [a,c,**]

[a] Center for Membrane and Water Science &Technology, Institute of Oceanic and Environmental Chemical Engineering, State Key Lab Breeding Base of Green Chemical Synthesis Technology, Zhejiang University of Technology, Hangzhou, 310014, PR China
[b] Hangzhou Special Equipments Inspection and Research Institute, Hangzhou, China
[c] College of Chemical Engineering and Material Science, Quanzhou Normal University, Quanzhou, 362000, China

ARTICLE INFO

Keywords:
$ZnO/Cu_2O/g\text{-}C_3N_4$ heterojunctions
Co-catalyst
Photocorrosion
Photocatalytic
Degradation of antibiotics

ABSTRACT

In view of the environmental pollution caused by antibiotics, the creation of an efficient photocatalytic material is an effectual way to carry out water remediation. Herein, we developed a smart strategy to synthesize $ZnO/Cu_2O/g\text{-}C_3N_4$ heterojunction photocatalysts for the photodegradation of hazardous antibiotics by one-pot synthesis method. In this system, the Cu_2O nanoparticles with electrons reducing capacity were coupled with $g\text{-}C_3N_4$ composites. The photocarriers were generated from the electric field of type I heterojunction between ZnO and $g\text{-}C_3N_4$ and type II heterojunction between Cu_2O and $g\text{-}C_3N_4$. ZnO as a co-catalyst was doped to $Cu_2O/g\text{-}C_3N_4$ catalyst system for removal of broad-spectrum antibiotics with the condition of visible light to protect Cu_2O from photocorrosion, which thereby accelerated photocatalytic reactivity. Benefiting by new p-n-n heterojunction, the resulting $ZnO/Cu_2O/g\text{-}C_3N_4$ composites had an excellent degradation performance of broad-spectrum antibiotics such as tetracycline (TC), chlortetracycline (CTC), oxytetracycline (OTC) and ciprofloxacin (CIP), the degradation of which were 98.79%, 99.5%, 95.35% and 73.53%. In particular, $ZnO/Cu_2O/g\text{-}C_3N_4$ photocatalysts showed a very high degradation rate of 98.79% for TC in first 30 min under visible light, which was 1.35 and 10.62 times higher than that of $Cu_2O/g\text{-}C_3N_4$ and $g\text{-}C_3N_4$, respectively. This work gives a fresh visual aspect for simultaneously solving the instability deficiencies of traditional photocatalysts and improving photocatalytic performance.

1. Introduction

Over last few decades, abuse use of antibiotics have led to a dramatical increase in antibiotic-resistant, which is a threat to people and animals [1, 2]. The traditional wastewater treatment can not meet the needs for the degradation of antibiotics. Therefore, a large amount of works to develop the new treatment technologies like biological method, Fenton reaction, electrodeposition and photocatalysis to degrade pollutants [3, 4]. In antibiotics disposal, photocatalytic process as an energy-saving and high efficiency technology has attracted a lot of attentions. Among numerous photocatalysts such as graphite carbon nitride ($g\text{-}C_3N_4$), titanium dioxide and bismuth(III) oxide [5, 6, 7], $g\text{-}C_3N_4$ as one of the most popular photocatalysts is used in the removing of broad-spectrum antibiotics owing to the unique structure of n-type nonmetallic semiconductor, thermodynamic stability and visible light absorption [8, 9]. However, the high recombination between electrons and holes and low visible light adsorption ability decrease the efficiency of the antibiotics elimination [10, 11].

In order to overcome this obstacle, many researchers are devoted to surface assembly by constructing heterojunction systems [12, 13]. According to transfer mechanism of $g\text{-}C_3N_4$ base heterostructure in photogenerated charge carriers, it can be grouped into: type-I heterojunction, type-II heterojunction, S-scheme heterojunction and Z-type heterojunction [14, 15, 16]. The narrow band gap about $g\text{-}C_3N_4$ would be improved through introducing another semiconductor photocatalysts and the visible light would be made the most of so as to achieve the high redox capability, fast photocarriers migration and space separation. Various metal oxides (TiO_2 [17], WO_3 [18], CeO_2 [19], In_2O_3 [20], MoO_3 [21], SnO_2 [22], Fe_2O_3 [23]), metal sulfides (CdS [24], ZnS [25], MoS_2 [26]), halides (BiOI [27], BiOCl [28], BiOBr [29], AgI [30], AgBr [31]), revised $g\text{-}C_3N_4$ and other semiconductors (such as Bi_2WO_6 [32], $BiPO_4$ [33], Ag_3PO_4 [34], SiC [35]) have been applied in forming customary

* Corresponding author.
** Corresponding author.
E-mail addresses: xuzehai520@163.com (Z. Xu), guoliangz@zjut.edu.cn (G. Zhang).

https://doi.org/10.1016/j.heliyon.2022.e12644
Received 13 June 2022; Received in revised form 27 October 2022; Accepted 19 December 2022

type II heterojunction systems based on g-C_3N_4. Among all metal oxide semiconductors, Cu_2O has drawn attention owing to its proper band position and good visible-light photocatalytic activity, when it acted as a typical p-type semiconductor to couple with a n-type semiconductor, formed heterojunction can specifically to broaden the photoabsorption area, improve photocatalysis performance and accelerate the valid separations of photocarriers [36, 37, 38]. The corresponding research confirmed that the progress on the production of hydrogen through combining Cu_2O with g-C_3N_4 to form type II heterojunction [39]. But this kind of photocatalytic agent are easily oxidized when produced electrons fail to remove them, so that it would be lose its chemical activity in the process of eliminating antibiotics. Therefore, a more smart strategy is needed to get much wider applications and have a more chemical stability after continual operation [40, 41, 42]. The three-phase heterojunction changes the rate-determining step and increases the catalytic rate. The synergy between carbon dots and heterojunctions could not only enhance light absorption range of semiconductor particles, but support separation of photogenerated charge carriers [43, 44]. Besides, Surface functionalization by incorporating some co-catalysts could facilitate the charge separation. Due to the energy level and electronic structure can match up with Cu_2O, ZnO is often used as co-catalysts [45, 46, 47]. Inspired by these concepts, we put forward an idea where the combination of ZnO co-catalyst and Cu_2O/g-C_3N_4 catalyst could be a feasible strategy to prepare high active heterojunction photocatalyst. There is no report on the preparation of highly active ZnO/Cu_2O/g-C_3N_4 heterojunction photocatalytic heterojunction for antibiotics removal so far.

In this work, we invented a facile way to produce ZnO/Cu_2O/g-C_3N_4 heterojunction photocatalysts by one-pot synthesis approach for the photodegradation of tetracycline. In this system, Cu_2O nanoparticles with electrons reducing capacity were connected with g-C_3N_4 composites. The photocarriers were generated from the electric field of type I heterojunction between ZnO and g-C_3N_4 and type II heterojunction between g-C_3N_4 and Cu_2O. Meanwhile, the ZnO particles as a co-catalyst became a transition place to accept more electrons, so that the photocorrrosion of Cu_2O was inhibited, and thereby accelerating photocatalytic reactivity. Moreover, ZnO as a co-catalyst to protect Cu_2O from photocorrosion. The photocatalytic activity, stability and possible mechanism of prepared ZnO/Cu_2O/g-C_3N_4 heterojunction were evaluated. The prepared ZnO/Cu_2O/g-C_3N_4 heterojunction exhibited good feasibility in absorbing visible light and could be applied in a variety of broad-spectrum antibiotics.

2. Experimental section

2.1. Materials

Copper chloride ($CuCl_2{\cdot}2H_2O$), citric acid ($C_6H_8O_7$), zinc nitrate ($Zn(NO_3)_2{\cdot}6H_2O$), sodium hydroxide (NaOH), ethanol, cetyltrimethylammonium bromide, polyvinylpyrrolidone (PVP), urea and ascorbic acid (AA) were bought from Sinopharm Chemical Reagents Co., Ltd. (Shanghai, China) and can be directly operated.

2.2. Preparation of g-C_3N_4 nanosheet

An alumina crucible with a lid filled with the urea as a precursor, and citric acid was added to promote polycondensation reaction. Then, mixed substance was heated to 500 °C for 1 h in the air, and the subsequent gray solid powder was g-C_3N_4 nanosheets [48, 49].

2.3. Preparation of ZnO nanorods

ZnO nanorods were synthesized by hydrothermal methods. In general, 0.079 g cetyltrimethylammonium bromide and 1.92 g NaOH were dissolved in 20 mL of deionized water, which was stirred to make a transparent solution. 2.32 g $Zn(NO_3)_2{\cdot}6H_2O$ was then introduced to above solution and vigorously stirred for 1h. Subsequently, the solution were transferred to reaction caldron under 90 °C for heating for 15 h. Finally, the ZnO was collected after centrifugation and drying.

2.4. Preparation of Cu_2O/g-C_3N_4 composites

Preparation of binary Cu_2O/g-C_3N_4 photocatalysts were made by a hydrothermal approach. The calculated amount of $CuCl_2{\cdot}2H_2O$ and NaOH aqueous solutions were first magnetic stirred at room temperature. After that, 0.2 g g-C_3N_4 powder was dispersed in the above mixed solution by rapid agitation. After stirring for 30 min, 0.01 M of ascorbic acid (AA) was put in the resultant above mixture and was stirred for 1 h. Eventually, powder was washed with ethanol before dried up in vacuum drying chamber at 30 °C for 24 h, so the collected ultimate production was labeled as Cu_2O/g-C_3N_4.

2.5. Preparation of ZnO/Cu_2O/g-C_3N_4 composite

Preparation of ternary ZnO/Cu_2O/g-C_3N_4 composites were made by a hydrothermal strategy (Figure 1). The preparation of ZnO/Cu_2O/g-C_3N_4 compound was same with the prepared Cu_2O/g-C_3N_4 except the addition of ZnO when the g-C_3N_4 composites were added. The resulting precipitate was centrifuged after the reaction, and was washed by ethanol and was added in a vacuum drying oven and then at 30 °C for 24 h. The final obtained product was called as ZnO/Cu_2O/g-C_3N_4 powder. For the convenience of description, the amount of ZnO added to obtain ZnO/Cu_2O/g-C_3N_4 composites were 5:1, 1:1 and 1:5, referred to as ZnO/Cu_2O/g–C_3N_4–1, ZnO/Cu_2O/g–C_3N_4–2, and ZnO/Cu_2O/g–C_3N_4–3, respectively.

2.6. Characterization

The chemical properties of the materials were observed by Fourier transform infrared (FT-IR) spectroscopy (Nicolet 6700, Thermo Scientific, USA). Scanning electron microscopy (SEM, TM-1000, Hitachi, Japan) characterizes the EDS elements and morphology of materials. At room temperature, the X'Pert PRO diffraction (Panalytical, Netherlands) observes the X-ray diffraction (XRD) patterns with Cu Ka radiation (40 kV, 40 mA, $\lambda = 0.154056$ nm). The X-ray photoelectron spectroscopy (XPS) was operated by PHI 5000C ESCA type and the X-ray source was Al Kα ray (hv = 1486.6 eV). The UV-vis DRS were performed on the Varian Cary 500 UV-Visible Diffuse Reflectometer of the American Company with high purity $BaSO_4$ as the standard reagent, with a scanning range of 200–800 nm and a scanning speed of 40 nm min^{-1}. TECNAI G2 F30 S-TWIN transmission electron microscope (TEM) was applied in studying surface morphology and particle size of the catalyst, and accelerating voltage was 300 kV. Bruker EMXPLUZ paramagnetic resonance spectrometer (ESR/EPR) was used to detect oxygen vacancies of free radicals and catalysts in photocatalytic degradation, and superoxide radicals ($\bullet O_2^-$) and hydroxyl radicals (•OH) were captured with 5,5-dimethyl-1-pyrroline-N-oxide (DMPO). The fluorescence intensity of catalyst was analyzed using the Edinburgh FLS1000 steady-state/transient fluorescence spectrometer (PL) and electrochemical impedance spectroscopy (EIS). Liquid chromatography Agilent 1290UPLC and mass spectrometry Agilent QTOF6550 were used to set up high performance liquid chromatography-tandem mass spectrometry (HPLC-MS) to analyze intermediates.

3. Results and discussion

X-ray diffraction (XRD) patterns of g-C_3N_4, Cu_2O/g-C_3N_4, and ZnO/Cu_2O/g-C_3N_4 are exhibited in Figure 2a. Representative peaks of Cu_2O at $2\theta = 36.5°$, 42.4°, 61.5° and 73.7° are matched with (111), (200), (220), and (311) crystal surface indexes of Cu_2O plane (JCPDS No. 78-2076), respectively [50]. g-C_3N_4 reveals two characteristic peaks (100) and (002) at $2\theta = 13.1°$ and 27.4°, individually, which is according to the

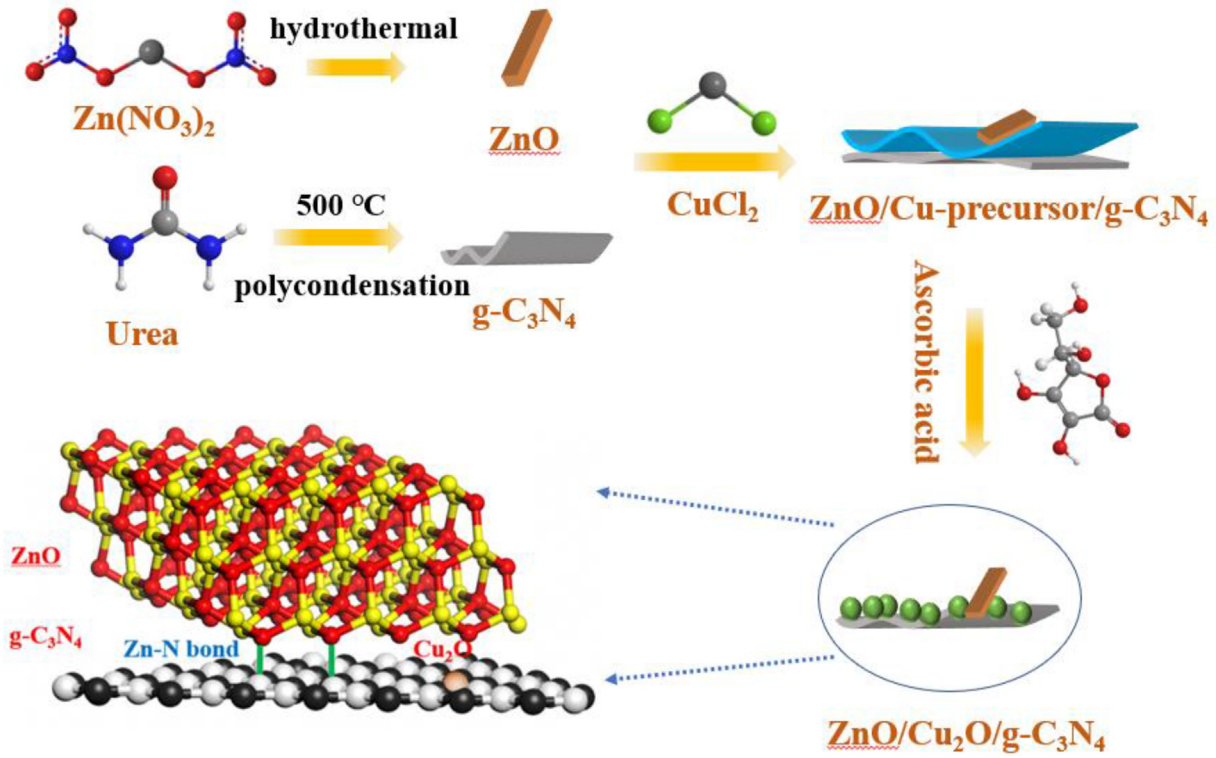

Figure 1. The process flow diagram of the preparation of g-C_3N_4/ZnO/Cu_2O photocatalysts.

simple aromatic ring and triazine stacking between layers [51]. In addition, the ZnO pattern shows three feature peaks at 31.8° (100), 34.4° (002) and 36.3° (101), in line with JCPDS No. 65-3411 [52,53]. Apparently, ZnO (★) and Cu_2O (●) coexist in the ZnO/Cu_2O/g-C_3N_4 sample, and the size of Cu_2O (14.5 nm) in the ZnO/Cu_2O/g-C_3N_4 photocatalyst was higher than the crystal size of Cu_2O (7.9 nm) in the Cu_2O/g-C_3N_4 catalyst through calculation of Scherrer formula. The addition of ZnO has an specific effect on the crystal size of Cu_2O. It demonstrates that Cu_2O in the ZnO/Cu_2O/g-C_3N_4 photocatalyst has better crystalline phase than Cu_2O in the Cu_2O/g-C_3N_4 photocatalyst, which reduces photocorrosion rate [54]. The Fourier Transform Infrared (FT-IR) spectroscopy of original g-C_3N_4, Cu_2O/g-C_3N_4, and ZnO/-Cu_2O/g-C_3N_4 compounds was observed in Figure 2b. Typical absorption peaks at 807 cm^{-1} and 890 cm^{-1} were connected with tri-s-triazine ring systems and the bending vibrations of N–H [55]. 1240 cm^{-1}, 1322 cm^{-1}, 1410 cm^{-1} and 1638 cm^{-1} characteristic peaks could affirm the presence of tensile vibrations of C–N and C=N, and the broader absorbing band of nearby 3167 cm^{-1} is connected with N–H and O–H vibrations [56]. Besides, the FT-IR spectrum of ternary ZnO/Cu_2O/g-C_3N_4 composite showed no obvious difference in the characteristic skeleton of the g-C_3N_4, confirming that ZnO and Cu_2O which were brought into is uninfluential in the initial structure of the g-C_3N_4 nanosheet, which is the same as the above XRD analysis outcomes.

The SEM and TEM results of the resulting ZnO/Cu_2O/g-C_3N_4 photocatalysts is observed in Figure 3. The microscopic test of g-C_3N_4 (Figure 3a) exhibits a uniform nanosheet two-dimensional flake structure. The appearance in Figure 3b, Figures 3d and Figure 3g exhibits a large number of Cu_2O nanoparticles with good adhesion stocking on the

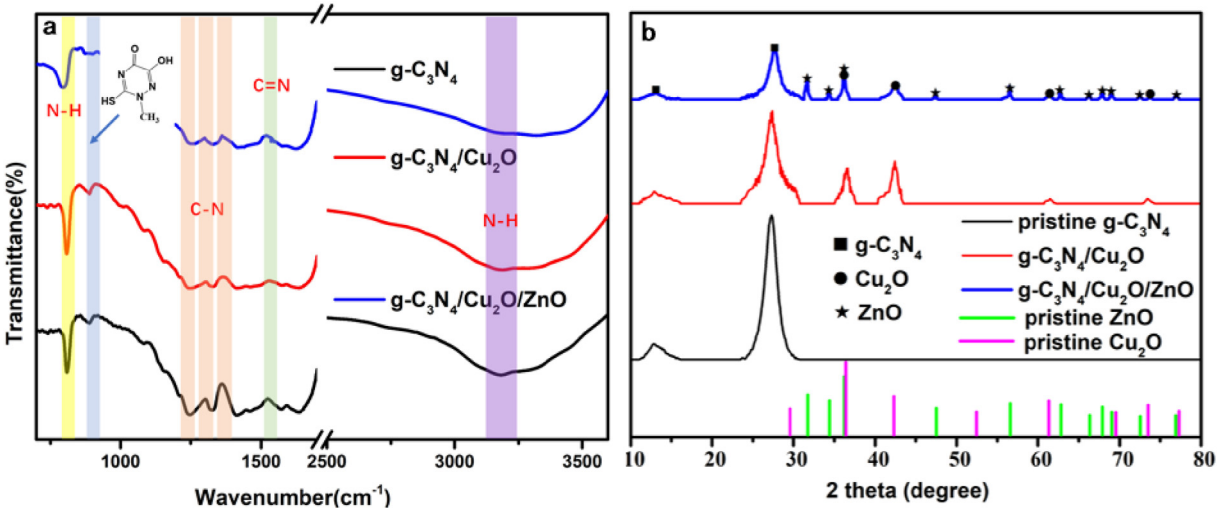

Figure 2. (a) XRD patterns and (b) FT-IR spectra of g-C_3N_4, g-C_3N_4/Cu_2O and g-C_3N_4/ZnO/Cu_2O photocatalysts.

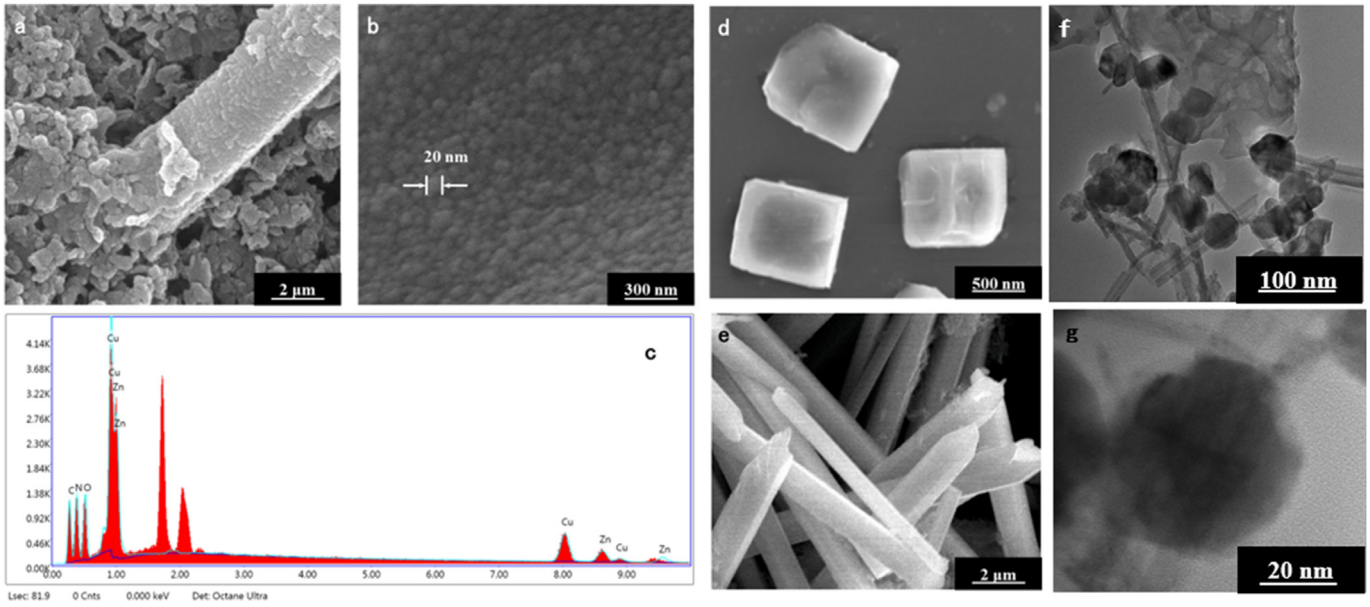

Figure 3. SEM images of (a, b) ZnO/Cu_2O/g-C_3N_4, (c) The EDS spectrum of ZnO/Cu_2O/g-C_3N_4, SEM images of (d, e) ZnO and Cu_2O and TEM images of (g, h) ZnO/Cu_2O/g-C_3N_4.

layer of g-C_3N_4. Meanwhile, as is vividly exhibited in Figure 3e and and Figure 3f, the pure ZnO prepared by hydrothermal method has a glossy nanorod surface topography. The EDS spectra of ZnO/Cu_2O/g-C_3N_4 is provided in Figure 3c, it can be obviously noticed that Zn, O, Cu, C and N elements consist of ZnO/Cu_2O/g-C_3N_4 compound catalyst. The atomic weight of Cu and Zn elements are measured by the peak area, which is a value of 12.26% and 6.30% respectively. It demonstrates the successful preparation of a ZnO/Cu_2O/g-C_3N_4 compound.

The X-ray photoelectron spectroscopy (XPS) is utilized to analyze and study composition of ZnO/Cu_2O/g-C_3N_4 in Figure 4a. The XPS spectrum of Cu 2p reveals two typical peaks in Figure 4b, which the Cu $2p_{3/2}$ and Cu $2p_{1/2}$ are found in the 932.05 eV and 952.0 eV, separately [57]. Furthermore, Figure 4c displays the two typical peaks of C 1s, the peaks at 284.35 eV and 287.55eV are related to the C=C sp^2 hybridized carbon in the structure of g-C_3N_4 and N–C=N sp^2 hybridization in the aromatic ring [58, 59]. In Figure 4d, binding energy of Zn 2p are detected in the 1020.65 eV and 1044.6 eV, which agrees with the Zn $2p_{3/2}$ and Zn $2p_{1/2}$, and is related to Zn^{2+} in ZnO [60, 61]. What's more, the spectrum of N 1s is separated into four peaks in Figure 4e. The peaks at about 398 eV, 398.8 eV, 400.3 eV, 404.2 eV are consistence with different combinations of N elements which includes C=N–C, N-$(C)_3$ groups, C–N(H)–C, Zn–N and π-excitation in the structure of g-C_3N_4 composites and ZnO

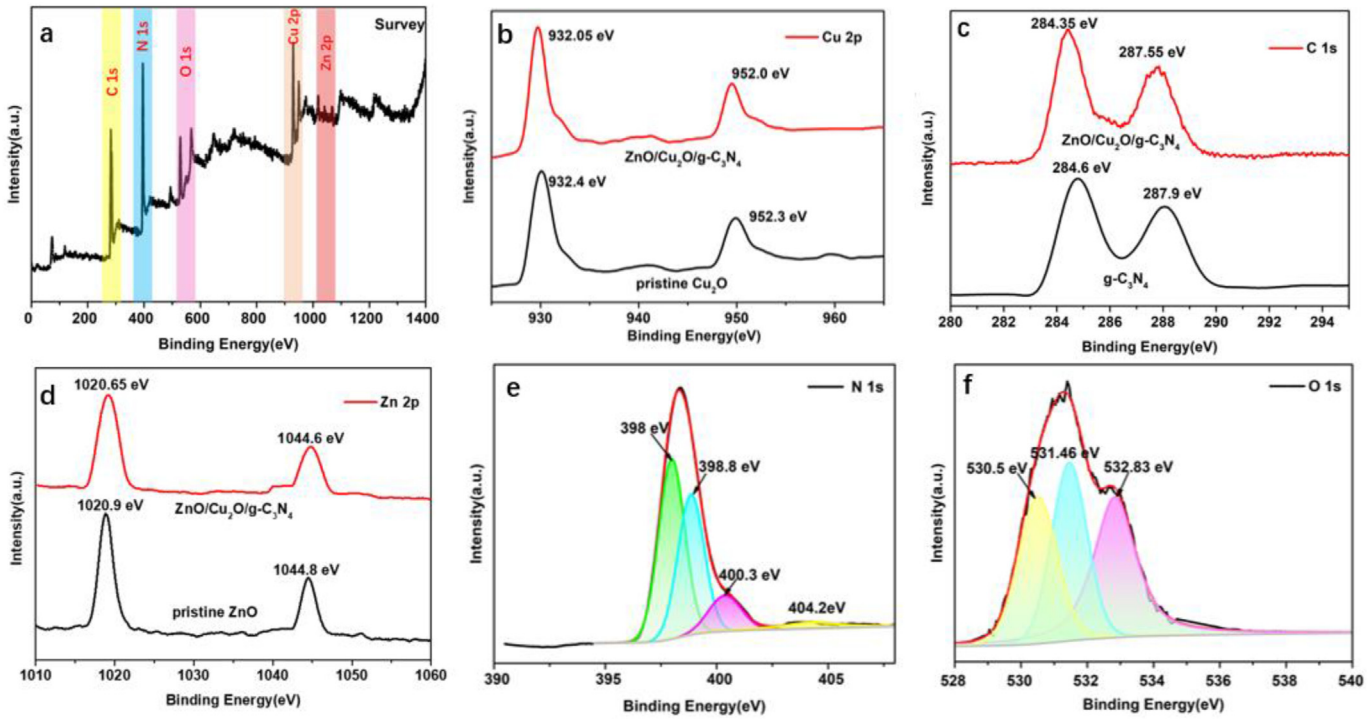

Figure 4. XPS spectra of (a) survey spectrum, (b) Cu 2p, (c) C 1s, (d) Zn 2p (e) N 1s (f) O 1s of ZnO/Cu_2O/g-C_3N_4 composites.

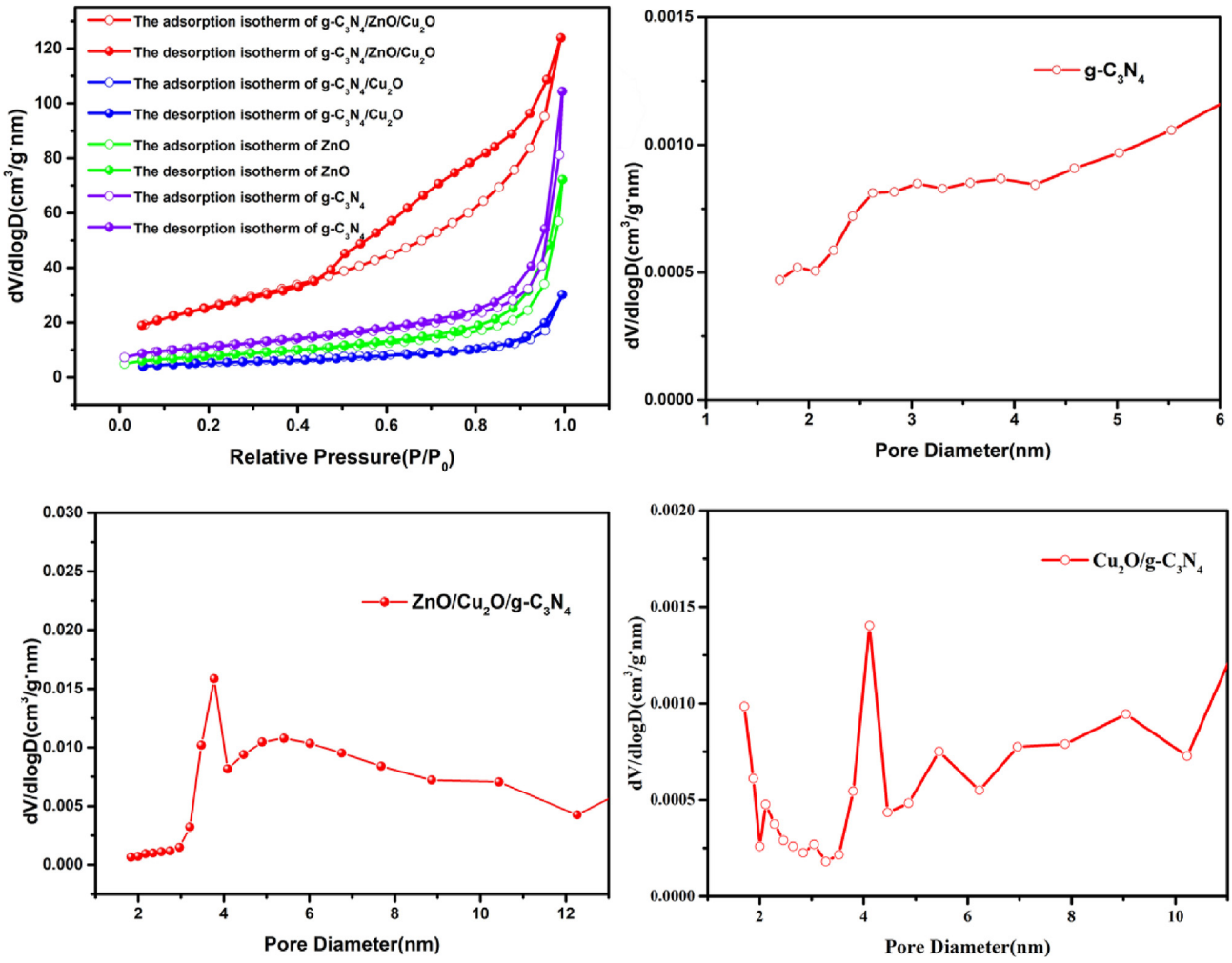

Figure 5. The N_2 adsorption-desorption isotherms and pore diameter of g-C_3N_4, ZnO, Cu_2O/g-C_3N_4 and ZnO/Cu_2O/g-C_3N_4 composite samples.

composites [58, 62]. Finally, Figure 4f shows three peaks of O 1s at 530.5 eV, 531.46 eV and 532.83 eV, which are linked with the existence of the weak binding of –OH, and the combination between O_2^- and the coactions of Cu/Zn [59, 63].

In addition, specific surface area and aperture distribution of photocatalysts are analyzed by using the BET surface area with N_2 adsorption-desorption isotherms which provides a more detailed basis for further analysis of the relation between the structure and properties of mesoporous material [64]. The calculation values of specific surface area Cu_2O/g-C_3N_4 and ZnO/Cu_2O/g-C_3N_4 ternary nanocomposites were 19.76 m^2/g and 93.372 m^2/g, individually (Figure 5). The BET measurement results of ZnO/Cu_2O/g-C_3N_4 nanocomposites was 4.73 times the height of Cu_2O/g-C_3N_4 samples. The porous Cu_2O/g-C_3N_4 composites exhibited a small specific surface area because the Cu_2O composites coat on the pore canal of g-C_3N_4 surface. The consequences show the higher surface area may promote more reaction sites to adsorb active substance and capture the charge carriers on its surface, which could be conducive to improving photocatalytic capability of ZnO/Cu_2O/g-C_3N_4 photocatalysts.

To study the optical properties and electrons transfer of photocatalytic materials, UV-vis absorption spectroscopy was utilized ranging 200–800 nm. As exhibited in Figure 6a, spectrographic absorption of original Cu_2O, g-C_3N_4, Cu_2O/g-C_3N_4 and ZnO/Cu_2O/g-C_3N_4 photocatalysts were collected. The g-C_3N_4 has an absorption edge near 200–410 nm due to electronic transition from N 2p to the C 2p orbit [65, 66]. Besides, the band energy (E_g) was measured by the method of Kubelka–Munk formula, and the value of Cu_2O, g-C_3N_4 and ZnO in Figures 6b, 6c and 6d were approximately 2.25 eV, 2.44 eV and 3.15 eV, which was consistence with preceding reports [36, 48, 66]. In addition, with the addition of ZnO and Cu_2O composites, absorption intensity of ZnO/Cu_2O/g-C_3N_4 heterostructure was expanded with the strongest visible light absorption zone of about 568 nm. These results showed that ZnO/Cu_2O/g-C_3N_4 ternary composites have higher visible light activity and much broader scale.

The photocatalytic activity of the prepared materials were measured by using visible light illumination toward target pollutants TC. Figure 7a shows the degradation dynamic curves of g-C_3N_4, Cu_2O/g-C_3N_4, and ZnO/Cu_2O/g-C_3N_4 composites. Before catalytic reaction, all the samples were subjected to dark adsorption experiments, and the absorbent equilibrium could be achieved after 30 min. Then results exhibited that ternary ZnO/Cu_2O/g-C_3N_4 photocatalyst had best photocatalytic performance (TC degradation rate of 98.79%) than that of original g-C_3N_4, Cu_2O, Cu_2O/g-C_3N_4. As depicted in the graph, pure g-C_3N_4 displayed the lowest absorption about visible light and separation speed about photogenerated carrier, leading to the lowest degradation performance of TC (only 9.24%). In addition, the degradation rate of the original Cu_2O was 58.36%, whose degradation was needed to improve. It is noteworthy that when Cu_2O/g-C_3N_4 is coupled, photocatalytic activity is increased and TC degradation efficiency of Cu_2O/g-C_3N_4 is 98.1% in first 1 h. Strikingly, when the ZnO co-catalyst was introduced into Cu_2O/g-C_3N_4 heterojunction systems, the photocatalytic ability of ternary ZnO/Cu_2O/g-C_3N_4 heterojunctions was significantly enhanced, all things being equal. Amazingly, ZnO/Cu_2O/g-C_3N_4 degrades TC at 30 min in visible light at a

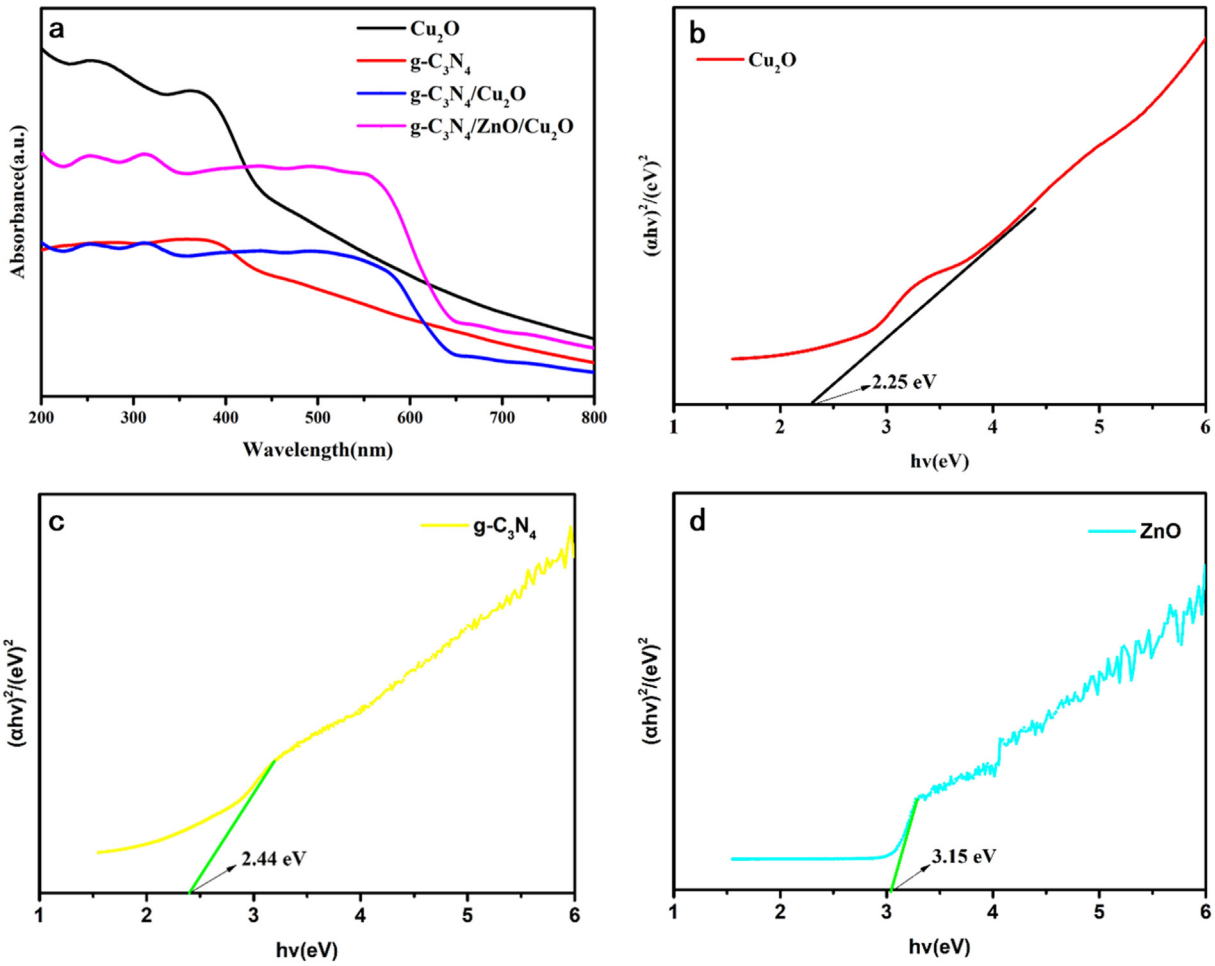

Figure 6. (a) UV-Vis DRS absorption spectra of g-C_3N_4, Cu_2O, Cu_2O/g-C_3N_4 and major ZnO/Cu_2O/g-C_3N_4 heterostructures.(b) band gap energy of g-C_3N_4, Cu_2O, ZnO.

rate of 98.79%. The increase of photocatalytic efficiency of ternary ZnO/Cu_2O/g-C_3N_4 composites is primarily due to the construction of p-n-n ZnO/Cu_2O/g-C_3N_4 ternary heterojunctions and the synergy between components. With the gradual increase of ZnO loading, photocatalytic efficiency of ternary composites diminish and the light shading effect is major reason.

The primary reaction kinetic equation was utilized to study the degradation law of the above photocatalysts [67], and thus the related ln(C_0/C) curve shows a good linear relationship (Figure 7b). What's more, the values of kinetics rate constant about all catalysts are revealed in a more visualized clearer line diagram. It is easy to see that the maximum rate constant of ZnO/Cu_2O/g-C_3N_4 is 0.0737 min^{-1}, which is about 49.13, 4.45 and 2.56 times the size of original g-C_3N_4, Cu_2O and Cu_2O/g-C_3N_4, respectively. It is worth noting that the comparison between this work and other previously reported ternary photocatalysts were shown in Table 1, and ZnO/Cu_2O/g-C_3N_4 photocatalytic materials displayed strong photocatalytic performance against degradation of pollutant TC together with visible light. Subsequently, OTC, CTC and CIP as other broad-spectrum antibiotics were selected to make further studies of prepared materials, as exhibited in Figure 7c. The photocatalytic degraded trend of antibiotics was similar to that of the above TC. Among them, the ternary ZnO/Cu_2O/g-C_3N_4 compound photocatalyst still shown best photocatalytic performance as a whole, which vividly indicated that the ternary ZnO/Cu_2O/g-C_3N_4 photocatalyst consisted of g-C_3N_4, ZnO and Cu_2O has much wider applications than others. Finally, for the sake of study the stability of the ZnO/-Cu_2O/g-C_3N_4 photocatalyst, it was explored again using a cyclic experiment under the same circumstances, as exhibited in Figure 7d. After four cycles, performance of photocatalytic degradation of TC almost did not decrease, which confirmed its superior stability. Meanwhile, the TEM images in Fig. S1 showed that no obvious change existed in the topography and size of the sample before and after the reaction. Besides, for further test structural stability after the reaction, XRD was carried out, Fig. S2 showed that the material remained structural integrity after cycling.

The major active substances in the degradation course of TC were determined by the capture experiment. In this process, triethanolamine, isopropanol (IPA) and p-benzoquinone were added to play a role as h^+, •OH, and $\bullet O_2^-$ scavengers in the degradation of TC. As can be known from Figures 8a and 8b, the degradation of TC was importantly inhibited with the appropriate addition of triethanolamine. What's more, introduction of p-benzoquinone had a considerable effect on inactivation of the ZnO/Cu_2O/g-C_3N_4 photocatalysts. The results of experiment showed h^+ and $\bullet O_2^-$ are main factor with the equal circumstances in the degradation of ZnO/Cu_2O/g-C_3N_4 composites.

Tetracycline hydrochlorides are a kind of amphoteric compounds, which consists of phenolic diketone moiety, dimethylammonium group and tricarbonyl system [68, 69]. Consequently, three structures are found including positively-charged ions (TCH_3^+) which exist in below 3.3, zwitter-ions existing between 3.3 and 7.7 (TCH_2) and negatively-charged ions (TCH^- or TCH_2^-) in the existence of above 7.7, as shown in Figure 9a [69]. Therefore, pH factor were operated by changing different pH values, and the degradation performance of TC consequently were discussed. Admittedly, •OH and $\bullet O_2^-$ were generated separately from holes and electrons [70, 71, 72]. However, the leading factors including $\bullet O_2^-$ and h^+ was confirmed by the scavenger photodegradation experiments in

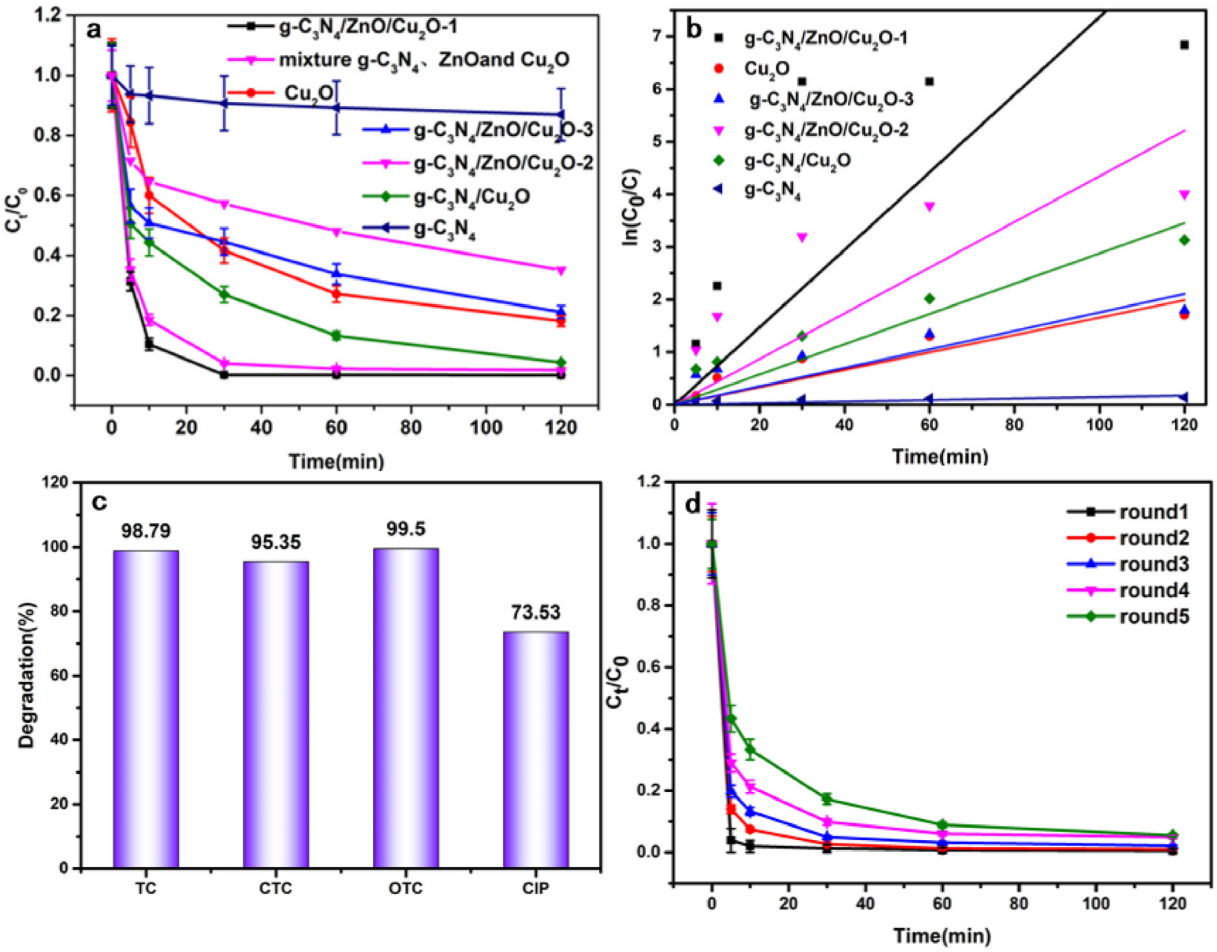

Figure 7. (a) Under visible light exposure ($\lambda > 420$ nm), TC is photodegraded on the prepared photocatalyst. (b) First-order dynamic plot. (c) The photodegradation test of the prepared photocatalyst was performed under visible light irradiation Antibiotics: over-the-counter, carbon tetrachloride and CIP. (d) Cyclic operation of photocatalytic TC degradation in the presence of $ZnO/Cu_2O/g\text{-}C_3N_4$ before and after 4 runs.

Table 1. Comparison of photocatalytic efficiencies of other previously reported ternary composite photocatalysts for degradation TC in recent years.

Samples	Catalyst gL^{-1}	CTC mgL^{-1}	Light source Xe lamp/W	DR%	Rate constant min^{-1}	References
$N\text{-GNDs/Ag/BiVO}_4$	0.5	20	300 ($\lambda > 420$ nm)	85.4 (80 min)	0.02433	[76]
$Ag_3PO_4/Co_3(PO_4)_2/g\text{-}C_3N_4$	0.5	10	300 ($\lambda > 420$ nm)	88 (120 min)	0.0159	[77]
$RGO/CdIn_2S_4/g\text{-}C_3N_4$	1.0	10	500 ($\lambda > 420$ nm)	74.02 (180 min)	0.00766	[78]
$BiOI@UIO\text{-}66(NH2)@g\text{-}C_3N_4$	0.2	20	300 ($\lambda > 420$ nm)	80 (180 min)	0.00851	[79]
$Bi_2O_3/Bi_2S_3/BaFe_{12}O_{19}$	1.0	5	300 ($\lambda > 420$ nm)	80 (15 min)	0.0264	[80]
$Ag@g\text{-}C_3N_4@BiVO_4$	0.3	20	300 ($\lambda > 420$ nm)	82.75 (60 min)	—	[81]
$Cu_3P/ZnSnO_3/g\text{-}C_3N_4$	0.5	10	500 ($\lambda > 420$ nm)	98.45% (60 min)	0.0543	[82]
$BiOI/g\text{-}C_3N_4/CeO_2$	0.5	20	300 ($\lambda > 420$ nm)	91.6 (120 min)	0.0205	[83]
$Ag/g\text{-}C_3N_4/SnS_2$	0.2	15	500 ($\lambda > 420$ nm)	94.9 (150 min)	0.0201	[84]
$Cu_2O/ZnO/g\text{-}C_3N_4$	0.5	20	350 ($\lambda > 420$ nm)	98.7 (30 min)	0.07372	This work

Figure 8a. Therefore, the detailed reactions would be shown in the following equation:

$$ZnO/Cu_2O/g\text{-}C_3N_4 + h\nu \rightarrow e^- + h^+ \quad (1)$$

$$e^- + O_2 \rightarrow \bullet O_2^- \quad (2)$$

$$\bullet O_2^- + H^+ \rightarrow \bullet HO_2 \rightarrow H_2O_2 \quad (3)$$

$$h^+/\bullet O_2^-/H_2O_2 + TC \rightarrow CO_2 + H_2O \quad (4)$$

As is vividly exhibited in Figure 9b and Table 2, degradation performance in the alkaline environment was stronger than that in acidity solution. Owing to the existence of $\bullet O_2^-$, rate constant was decreased from 0.0737 min^{-1} to 0.0295 min^{-1} by changing pH from 4 to 7. These results was demonstrated that $\bullet O_2^-$ really stimulated a good photodegradation response.

What's more, the existence of co-existing ions were researched to get better evaluations as a result of the complexity of wastewater. In general, the positive ions like Na^+、Mg^{2+}、K^+、Zn^{2+} have a little impact on the degradation performance in Figure 9c because these ions are fail to compete with catalysts and even enhance the conductivity. Meanwhile, the introduction of NO_2^- was different from other negative ions including Cl^-、NO_3^-、SO_4^{2-} in Figure 9d. It has a significantly lower efficiency due

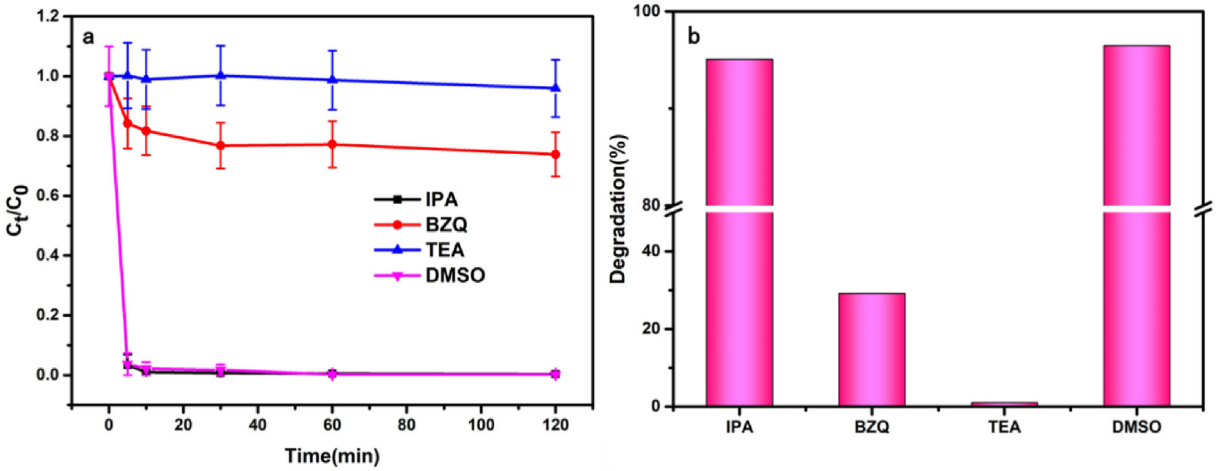

Figure 8. Photocatalytic activity of ZnO/Cu_2O/g-C_3N_4 composites on TC degradation under different quenching conditions.

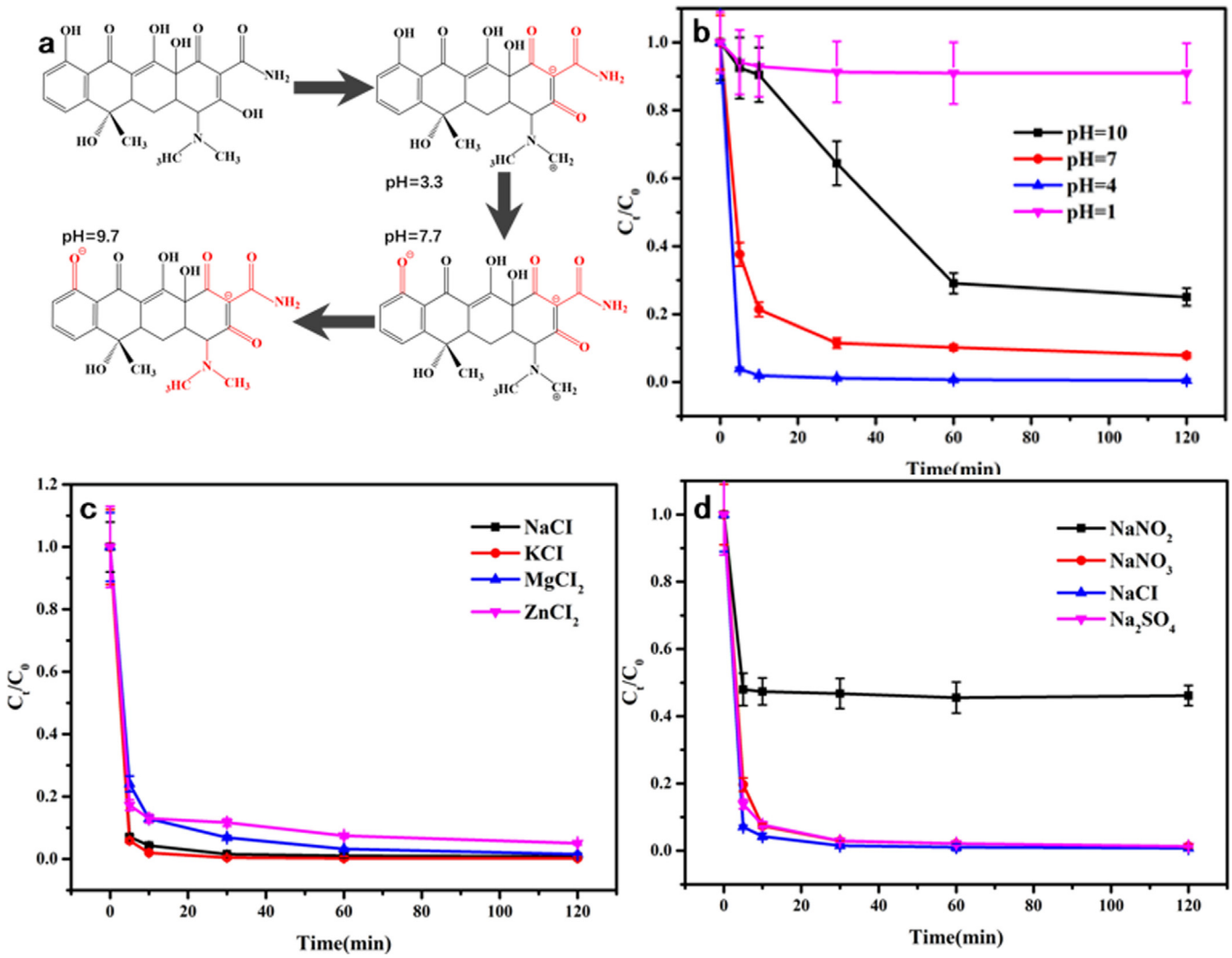

Figure 9. (a) Molecular structure of TC under different pH. The photodegradation test of the prepared photocatalyst was performed under visible light irradiation Antibiotics: (b) The effect of variable pH values. (c) The effect of different positive ions. (d) The effect of different negative ions.

to the NO_2^- ions suffering competition with tetracycline hydrochlorides. NO_2^- ions tended to be oxidized by the $\bullet O_2^-$ and the photodegradation consequently was lower.

High performance liquid chromatography (HPLC)-mass spectrometry (MS) was applied in revealing for complete pathway of TC photocatalytic oxidation. Photocatalytic oxidation $\cdot O_2^-$ free radicals attack the double

Table 2. The kinetic parameter of different photocatalysts in the degradation of TC.

Samples	TC (mgL^{-1})	K(min^{-1})	R^2
g-C_3N_4	40	0.0015	0.96
Cu_2O	40	0.0166	0.90
Cu_2O/g-C_3N_4	40	0.0288	0.90
ZnO/Cu_2O/g–C_3N_4–1	40	0.0737	0.91
ZnO/Cu_2O/g–C_3N_4–2	40	0.0435	0.94
ZnO/Cu_2O/g–C_3N_4–3	40	0.0176	0.94

bonds, phenol groups and amine groups of TC, and generate different intermediates m/z = 476.3, 396.8 and 229.2 in 4.496min, 5.770min and 6.843min, and finally generate CO_2 and H_2O in Figure 10. Based on detected intermediates, the degradation pathway associated with TC is inferred as shown in Figure 11 [73].

According to test data of valence band X-ray photoelectron spectroscopy (VB XPS), obtained pattern is extrapolated to the intersection of horizontal extension line around 0 eV, and the intersection point is E_v. As shown in Figure 12, according to the VB XPS maps of g-C_3N_4, Cu_2O and ZnO, a straight line is found to be extended near 0 eV, and the intersection point is the valence band position energy obtained by extending the horizontal part less than 0 eV. Therefore, valence band positions of g-C_3N_4, Cu_2O and ZnO correspond to energies of 1.6 eV, 1 eV and 2 eV, respectively. Therefore, the values of E_v and E_c of g-C_3N_4, Cu_2O and ZnO composites was deduced and photocatalytic mechanism of ZnO/Cu_2O/g-C_3N_4 heterojunctions are shown in Figure 14 [39].

Electrochemical impedance spectroscopy tests were applied in knowing charge transfer behavior, and results were shown in Figure 13a.

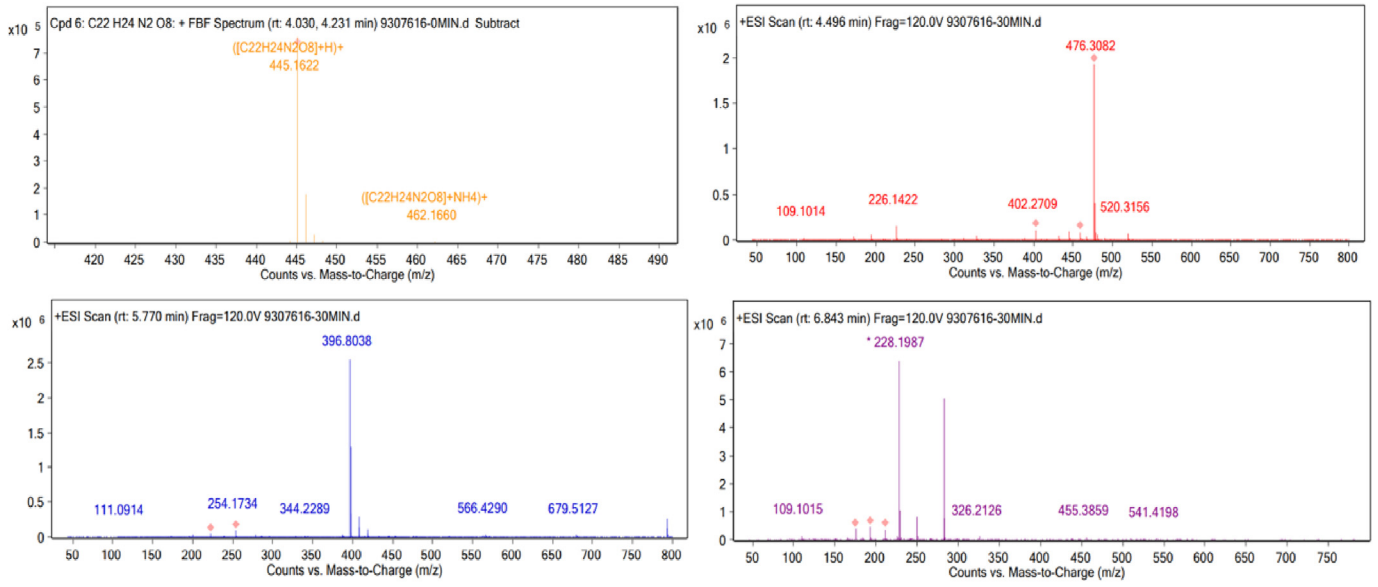

Figure 10. HPLC-MS of the degradation of TC with ZnO/Cu_2O/g-C_3N_4 catalyst at different times.

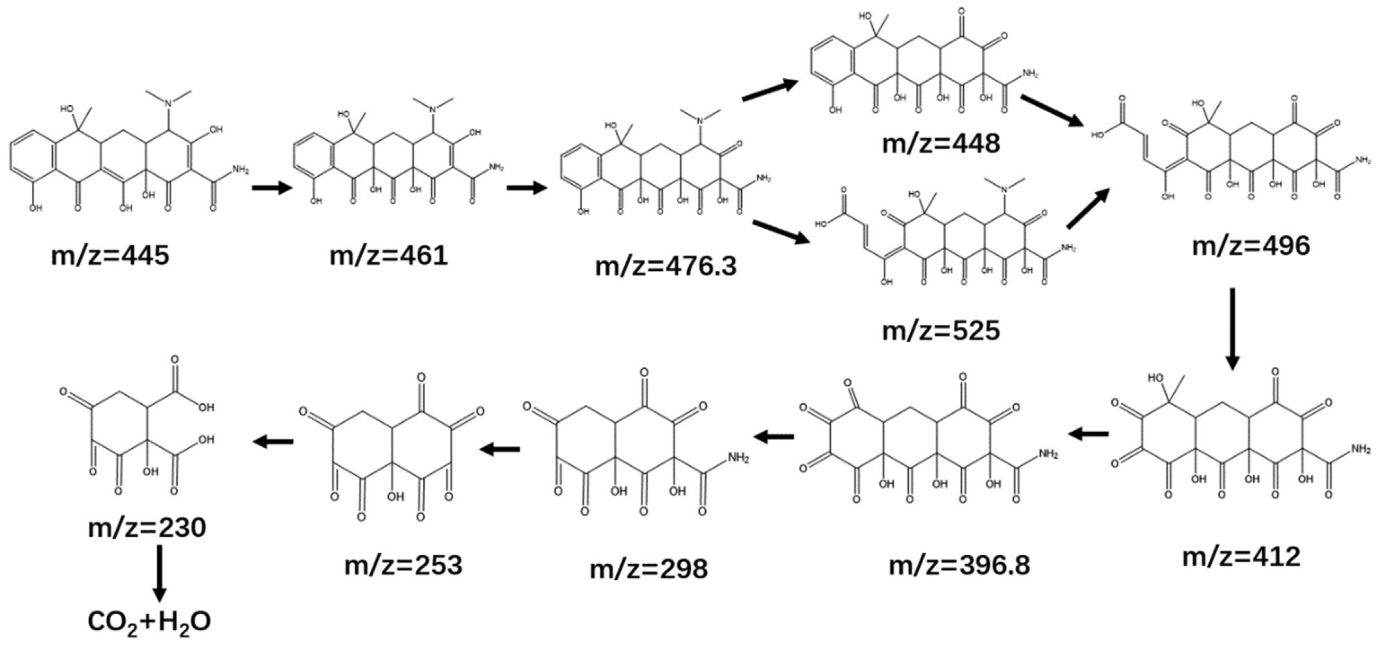

Figure 11. Possible TC degradation pathways.

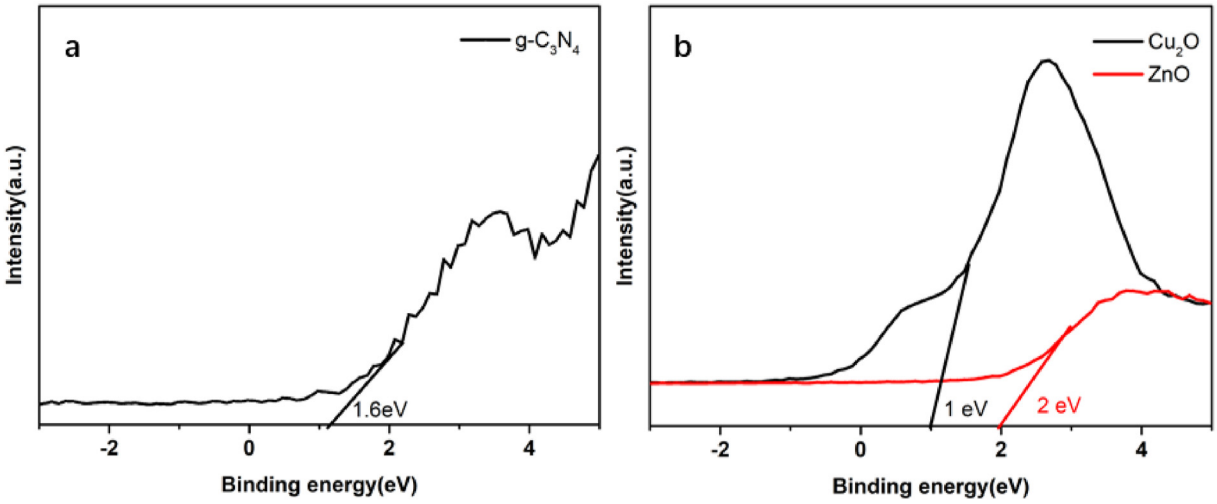

Figure 12. Valence band X-ray photoelectron spectroscopy: (a) g-C_3N_4, (b) ZnO and Cu_2O.

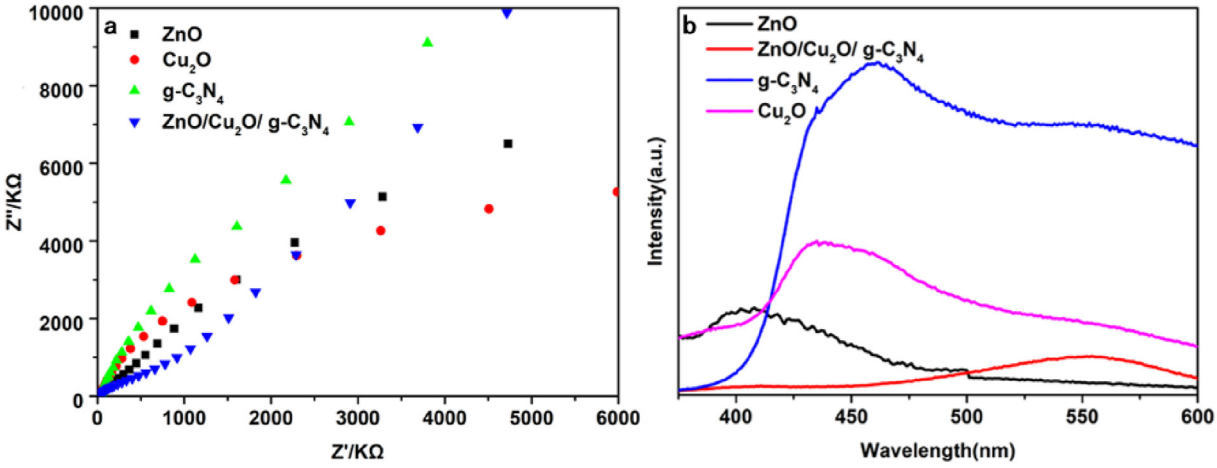

Figure 13. (a) EIS response and (b) photoluminescence spectra of g-C_3N_4, Cu_2O, ZnO and ZnO/Cu_2O/g-C_3N_4 materials.

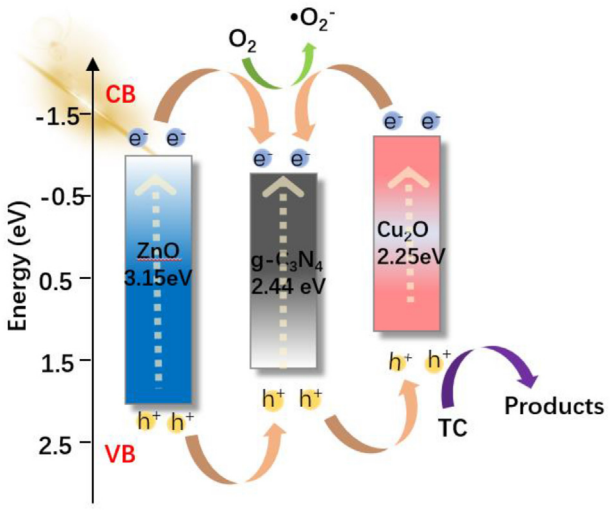

Figure 14. Photocatalytic mechanism of ZnO/Cu_2O/g-C_3N_4 p-n-n heterojunctions.

ZnO/Cu_2O/g-C_3N_4 had the smallest radius of arc and resistance, denoting the preparation of ZnO/Cu_2O/g-C_3N_4 composites could effectually cut the transfer resistance of interfacial charge from electrode to electrolyte molecule, promoting the efficient transport and separation between photogenerated carriers [75]. Besides, the electron-hole pairs of ZnO, g-C_3N_4, Cu_2O and ZnO/Cu_2O/g-C_3N_4 in the separation efficiency was analyzed by photoluminescence spectroscopy in Figure 13b. Admittedly, higher fluorescence intensity shows greater recombination of electron-hole. Due to electron-hole pairs excited by light absorption are recombined in large quantities, g-C_3N_4 had the highest the PL peak intensity. ZnO/Cu_2O/g-C_3N_4 had much lower PL peak intensities than other catalysts, denoting that hole and electron recombination was inhibited. Therefore, the photoelectric performance about ZnO/-Cu_2O/g-C_3N_4 was noticeably superior than that about single-phase materials, denoting the prominent photocatalytic performance.

In order to confirm the mechanism of electron transport between three materials among Cu_2O, g-C_3N_4 and ZnO, DMPO was used as the self-selected trapping agent of active free radicals in the electron spin resonance spectroscopy (ESR) to determine free radical generation. Under the condition of dark, ZnO/Cu_2O/g-C_3N_4 didn't produce any free radical signals, while after visible light irradiation DMPO ·OH appeared in Figure 15a. The OH signal was particularly weak because the ZnO with VB of 2 eV was dispersed to VB of 1.6 eV of g-C_3N_4, which was inferior to the generation potential of hydroxyl radicals(the value of H_2O/·OH is 1.99 eV) [74]. As exhibited in Figure 15b, ZnO/Cu_2O/g-C_3N_4 did not produce any free radical signals under dark conditions, and a strong DMPO ·O_2^- appeared after visible light irradiation, which was due to the CB values of g-C_3N_4 (−0.84 eV) and Cu_2O (−1.25 eV) were higher than

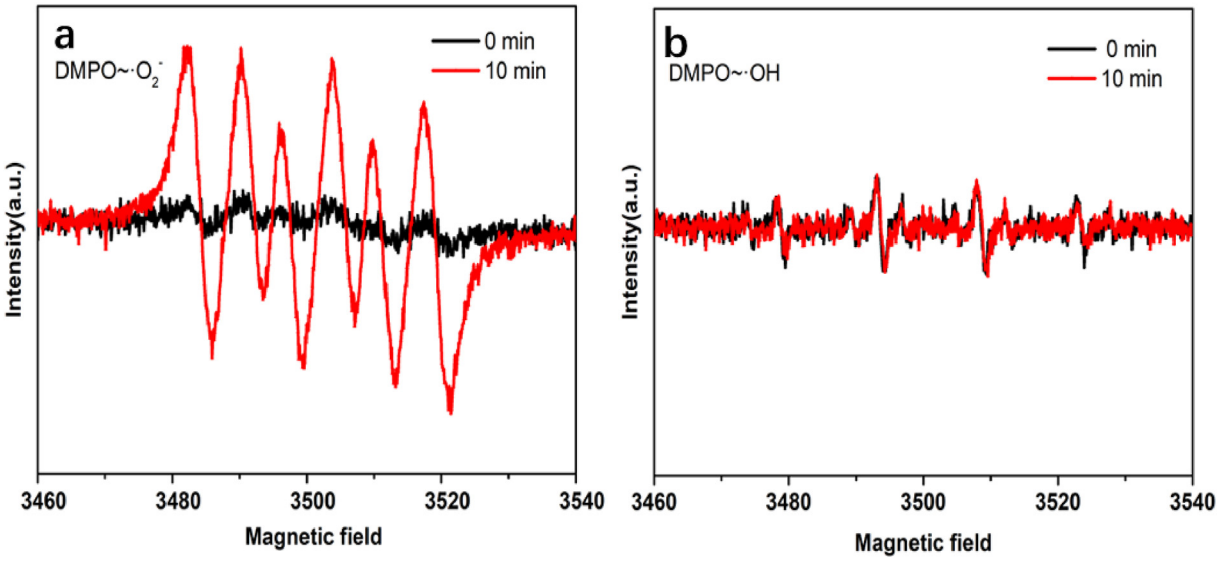

Figure 15. ESR spectra of (a) DMPO ·OH of ZnO/Cu_2O/g-C_3N_4. (b) DMPO ·O_2^- of ZnO/Cu_2O/g-C_3N_4.

the potential for superoxide radical generation ($O_2/\cdot O_2^-$ = -0.33 eV) [75].

The Fermi level (EF) of n-type ZnO and p-type Cu_2O semiconductors is close to that of Electronic Valence Band, whereas the EF of n-type ZnO and g-C_3N_4 semiconductors is near Electronic Conduct Band. Strikingly, when the photogenerated carriers of ZnO/Cu_2O/g-C_3N_4 photocatalyst are transferred with using visible light due to typical heterojunction mechanism, photogenerated electrons on the CB of ZnO and Cu_2O are transported to the conduct band of g-C_3N_4, and the holes are generated on the ZnO and g-C_3N_4's VB and which are transported on the valence band of Cu_2O. The VB of g-C_3N_4 in visible light is used to catch and restore O_2 to $\bullet O_2^-$ to minish the concentration of antibiotics, when h^+ on the VB of Cu_2O will directly break down the antibiotics into other products, which is type II heterojunction between g-C_3N_4 and Cu_2O and type I heterojunction between g-C_3N_4 and ZnO. The mechanism of band gap is logical, which is correspond with the results of the experimental catch, further demonstrating the reasonability of the p-n-n heterojunction theory. Based on above results, the ZnO/Cu_2O/g-C_3N_4 heterojunction composite photocatalyst successfully realized high rate of photogenerated electrons separation on the contact of interface, and thus material removal efficiency of pollutants was improved in water.

4. Conclusion

In summary, ZnO/Cu_2O/g-C_3N_4 p-n-n type heterogeneous composite was successfully synthesized by an uncomplicated and effortless hydrothermal approach. The photocarriers were generated from the electric field of type I heterojunction between g-C_3N_4 and ZnO and type II heterojunction between g-C_3N_4 and Cu_2O. Meanwhile, the ZnO particles as a co-catalyst became a transition place to accept more electrons, so that the photocorrrosion of Cu_2O was inhibited, thus accelerating photocatalytic reactivity. On account of the advantages of the internal electric field derived from heterojunction system, photogenerated electron-hole pairs could be quickly separated and transported in ternary ZnO/Cu_2O/g-C_3N_4 heterojunction. Besides, compared to pure catalysts and binary composites, photocatalytic antibiotic activity was largely enhanced with the condition of visible light. As a result, ZnO/Cu_2O/g-C_3N_4 revealed a very high degradation rate of 98.79% for TC in first 30 min under visible light, which was 1.35 and 10.62 times the height of Cu_2O/g-C_3N_4 and g-C_3N_4, respectively. The produced p-n-n heterojunction photocatalyst may give a fresh viewpoint in the area of designing photocatalysts with progressive structures and high performance in the water remediation.

Declarations

Author contribution statement

Yujie Zhu: Conceived and designed the experiments; Performed the experiments; Analyzed and interpreted the data; Contributed reagents, materials, analysis tools or data; Wrote the paper.

Ling Wang, Wentao Xu, Junsheng Yuan: Analyzed and interpreted the data.

Zehai Xu: Conceived and designed the experiments; Analyzed and interpreted the data; Contributed reagents, materials, analysis tools or data; Wrote the paper.

Guoliang Zhang: Conceived and designed the experiments; Contributed reagents, materials, analysis tools or data.

Funding statement

Dr. Zehai Xu and Guoliang Zhang National Natural Science Foundation of China (21808202 & 21736009).

Data availability statement

Data will be made available on request.

Declaration of interests statement

The authors declare no competing interests.

Additional information

Supplementary content related to this article has been published online at https://doi.org/10.1016/j.heliyon.2022.e12644.

References

[1] E. Evgenidou, Z. Chatzisalata, A. Tsevis, K. Bourikas, P. Torounidou, D. Sergelidis, A. Koltsakidou, D.A. Lambropoulou, Photocatalytic degradation of a mixture of eight antibiotics using Cu-modified TiO_2 photocatalysts: kinetics, mineralization, antimicrobial activity elimination and disinfection, J. Environ. Chem. Eng. 9 (2021), 105295.

[2] C.G. Li, Q. Tian, Y.L. Zhang, Y.Y. Li, X.M. Yang, H. Zheng, L.Y. Chen, F.M. Li, Sequential combination of photocatalysis and microalgae technology for promoting the degradation and detoxification of typical antibiotics, Water Res. 210 (2022), 117985.

[3] L. Qin, R. Ru, J.W. Mao, Q. Meng, Z. Fan, X. Li, G.L. Zhang, Assembly of MOFs/polymer hydrogel derived Fe_3O_4-CuO@hollow carbon spheres for photochemical oxidation: freezing replacement for structural adjustment, Appl. Catal., B 269 (2020), 118754.

[4] Z.H. Xu, C. Huang, L. Wang, X.X. Pan, L. Qin, X.W. Guo, G.L. Zhang, Sulfate functionalized Fe_2O_3 nanoparticles on TiO_2 nanotube as efficient visible light-active photo-fenton catalyst, Ind. Eng. Chem. Res. 54 (2015) 4593–4602.

[5] R. Tang, D. Gong, Y. Deng, S. Xiong, J. Zheng, L. Li, Z. Zhou, L. Su, J. Zhao, pi-pi stacking derived from graphene-like biochar/g-C_3N_4 with tunable band structure for photocatalytic antibiotics degradation via peroxymonosulfate activation, J. Hazard Mater. 423 (2022), 126944.

[6] A.Y. Meng, B.C. Zhu, B. Zhong, L.Y. Zhang, B. Cheng, Direct Z-scheme TiO_2/CdS hierarchical photocatalyst for enhanced photocatalytic H_2-production activity, Appl. Surf. Sci. 422 (2017) 518–527.

[7] E. Luevano-Hipolito, L.M. Torres-Martinez, L.V.F. Cantu-Castro, Self-cleaning coatings based on fly ash and bismuth-photocatalysts: Bi_2O_3, $Bi_2O_2CO_3$, BiOI, $BiVO_4$, $BiPO_4$, Construct. Build. Mater. 220 (2019) 206–213.

[8] H.X. Fang, H. Guo, C.G. Niu, C. Liang, D.W. Huang, N. Tang, H.Y. Liu, Y.Y. Yang, L. Li, Hollow tubular graphitic carbon nitride catalyst with adjustable nitrogen vacancy: enhanced optical absorption and carrier separation for improving photocatalytic activity, Chem. Eng. J. 402 (2020), 126185.

[9] X. Hu, Y. Yu, D. Chen, W. Xu, J. Fang, Z. Liu, R. Li, L. Yao, J. Qin, Z. Fang, Anatase/Rutile homojunction quantum dots anchored on g-C_3N_4 nanosheets for antibiotics degradation in seawater matrice via coupled adsorption-photocatalysis: mechanism insight and toxicity evaluation, Chem. Eng. J. 432 (2022), 134375.

[10] S. Chen, Y. Hu, S. Meng, X. Fu, Study on the separation mechanisms of photogenerated electrons and holes for composite photocatalysts g-C_3N_4-WO_3, Appl. Catal., B 150–151 (2014) 564–573.

[11] J. Zhao, N. Li, R. Yu, Z. Zhao, J. Nan, Magnetic field enhanced denitrification in nitrate and ammonia contaminated water under 3D/2D Mn_2O_3/g-C_3N_4 photocatalysis, Chem. Eng. J. 349 (2018) 530–538.

[12] Y. Zhang, C. Chai, X.C. Zhang, J.X. Liu, D.H. Duan, C.M. Fan, Y.F. Wang, Construction of Pt-decorated g-C_3N_4/Bi_2WO_6 Z-scheme composite with superior solar photocatalytic activity toward rhodamine B degradation, Inorg. Chem. Commun. 100 (2019) 81–91.

[13] S.Q. Zhang, Z.F. Zhang, B. Li, W.L. Dai, Y.M. Si, L.X. Yang, S.L. Luo, Hierarchical Ag_3PO_4@$ZnIn_2S_4$ nanoscoparium: an innovative Z-scheme photocatalyst for highly efficient and predictable tetracycline degradation, J. Colloid Interface Sci. 586 (2021) 708–718.

[14] Y.F. Li, M.H. Zhou, B. Cheng, Y. Shao, Recent advances in g-C_3N_4-based heterojunction photocatalysts, J. Mater. Sci. Technol. 56 (2020) 1–17.

[15] S.J. Li, M.J. Cai, Y.P. Liu, C.C. Wang, R.Y. Yan, X.B. Chen, Constructing $Cd_{0.5}Zn_{0.5}S$/Bi_2WO_6 S-scheme heterojunction for boosted photocatalytic antibiotic oxidation and Cr(VI) reduction, Appl. Surf. Sci. 610 (2022), 155346.

[16] J.X. Low, J.G. Yu, M. Jaroniec, S. Wageh, A.A. Al-Ghamdi, Heterojunction photocatalysts, Adv. Mater. 29 (2017), 1601694.

[17] K. Sridharan, E. Jang, T.J. Park, Novel visible light active graphitic C_3N_4-TiO_2 composite photocatalyst: synergistic synthesis, growth and photocatalytic treatment of hazardous pollutants, Appl. Catal., B 142 (2013) 718–728.

[18] R.X. Zhao, X.P. Li, J.X. Su, X.H. Gao, Preparation of WO_3/g-C_3N_4 composites and their application in oxidative desulfurization, Appl. Surf. Sci. 392 (2017) 810–816.

[19] N. Tian, H.W. Huang, C.Y. Liu, F. Dong, T.R. Zhang, X. Du, S.X. Yu, Y.H. Zhang, In situ co-pyrolysis fabrication of CeO_2/g-C_3N_4 n-n type heterojunction for synchronously promoting photo-induced oxidation and reduction properties, J. Mater. Chem. 3 (2015) 17120–17129.

[20] M.M. Sun, Z.Y. Chen, Y.Y. Bu, Enhanced photoelectrochemical cathodic protection performance of the C_3N_4@In_2O_3 nanocomposite with quasi-shell-core structure under visible light, J. Alloys Compd. 618 (2015) 734–741.

[21] L.Y. Huang, H. Xu, R.X. Zhang, X.N. Cheng, J.X. Xia, Y.G. Xu, H.M. Li, Synthesis and characterization of g-C_3N_4/MoO_3 photocatalyst with improved visible-light photoactivity, Appl. Surf. Sci. 283 (2013) 25–32.

[22] F. Raziq, Y. Qu, M. Humayun, A. Zada, H.T. Yu, L.Q. Jing, Synthesis of SnO_2/B-P codoped g-C_3N_4 nanocomposites as efficient cocatalyst-free visible-light photocatalysts for CO_2 conversion and pollutant degradation, Appl. Catal., B 201 (2017) 486–494.

[23] K.C. Christoforidis, T. Montini, E. Bontempi, S. Zafeiratos, J.J.D. Jaen, P. Fornasiero, Synthesis and photocatalytic application of visible-light active beta-Fe_2O_3/g-C_3N_4 hybrid nanocomposites, Appl. Catal., B 187 (2016) 171–180.

[24] Q.J. Fan, Y.N. Huang, C. Zhang, J.J. Liu, L.Y. Piao, Y.C. Yu, S.L. Zuo, B.S. Li, Superior nanoporous graphitic carbon nitride photocatalyst coupled with CdS quantum dots for photodegradation of RhB, Catal. Today 264 (2016) 250–256.

[25] B. Xue, H.Y. Jiang, T. Sun, F. Mao, ZnS@g-C_3N_4 composite photocatalysts: in situ synthesis and enhanced visible-light photocatalytic activity, Catal. Lett. 146 (2016) 2185–2192.

[26] J.J. Wang, Z.Y. Guan, J. Huang, Q.X. Li, J.L. Yang, Enhanced photocatalytic mechanism for the hybrid g-C_3N_4/MoS_2 nanocomposite, J. Mater. Chem. 2 (2014) 7960–7966.

[27] J. Di, J.X. Xia, S. Yin, H. Xu, L. Xu, Y.G. Xu, M.Q. He, H.M. Li, Preparation of sphere-like g-C_3N_4/BiOI photocatalysts via a reactable ionic liquid for visible-light-driven photocatalytic degradation of pollutants, J. Mater. Chem. 2 (2014) 5340–5535.

[28] F. Chang, Y.C. Xie, J. Zhang, J. Chen, C.L. Li, J. Wang, J.R. Luo, B.Q. Deng, X.F. Hu, Construction of exfoliated g-C_3N_4 nanosheets-BiOCl hybrids with enhanced photocatalytic performance, RSC Adv. 4 (2014) 28519–28528.

[29] J. Fu, Y.L. Tian, B.B. Chang, F.N. Xi, X.P. Dong, BiOBr-carbon nitride heterojunctions: synthesis, enhanced activity and photocatalytic mechanism, J. Mater. Chem. 22 (2012) 21159–21166.

[30] L. Liu, Y.H. Qi, J.Y. Yang, W.Q. Cui, X.G. Li, Z.S. Zhang, An AgI@ g-C_3N_4 hybrid core@shell structure: stable and enhanced photocatalytic degradation, Appl. Surf. Sci. 358 (2015) 319–327.

[31] S.Y. Yang, W.Y. Zhou, C.Y. Ge, X.T. Liu, Y.P. Fang, Z.S. Li, Mesoporous polymeric semiconductor materials of graphitic-C_3N_4: general and efficient synthesis and their integration with synergistic AgBr NPs for enhanced photocatalytic performances, RSC Adv. 3 (2013) 5631–5638.

[32] W.J. Yin, S. Bai, Y.J. Zhong, Z.Q. Li, Y. Xie, Direct generation of fine Bi_2WO_6 nanocrystals on g-C_3N_4 nanosheets for enhanced photocatalytic activity, Chem. Nano. Mat. 2 (2016) 732–738.

[33] C.S. Pan, J. Xu, Y.J. Wang, D. Li, Y.F. Zhu, Dramatic activity of C_3N_4/$BiPO_4$ photocatalyst with core/shell structure formed by self-assembly, Adv. Funct. Mater. 22 (2012) 1518–1524.

[34] L. Liu, Y.H. Qi, J.R. Lu, S.L. Lin, W.J. An, Y.H. Liang, W.Q. Cui, A stable Ag_3PO_4@g-C_3N_4 hybrid core@shell composite with enhanced visible light photocatalytic degradation, Appl. Catal., B 183 (2016) 133–141.

[35] B. Wang, J.T. Zhang, F. Huang, Enhanced visible light photocatalytic H_2 evolution of metal-free g-C_3N_4/SiC heterostructured photocatalysts, Appl. Surf. Sci. 391 (2017) 449–456.

[36] A. Khakzad, A. Ebrahimian Pirbazari, F. Esmaeili Khalil Saraei, M.A. Aroon, Combination of Cu_2O semiconductor with reduced graphene oxide nanocomposites for boosting photocatalytic performance in degradation of organic pollutant, Phys. B Condens. Matter 603 (2021), 412736.

[37] P.S. Selvamani, J.J. Vijaya, L.J. Kennedy, A. Mustafa, M. Bououdina, P.J. Sophia, R.J. Ramalingam, Synergic effect of Cu_2O/MoS_2/rGO for the sonophotocatalytic degradation of tetracycline and ciprofloxacin antibiotics, Ceram. Int. 47 (2021) 4226–4237.

[38] L.S. Lin, T. Huang, J. Song, X.Y. Ou, Z. Wang, H. Deng, R. Tian, Y. Liu, J.F. Wang, Y. Liu, G. Yu, Z. Zhou, S. Wang, G. Niu, H.H. Yang, X. Chen, Synthesis of copper peroxide nanodots for H_2O_2 self-supplying chemodynamic therapy, J. Am. Chem. Soc. 141 (2019) 9937–9945.

[39] K. Zhang, Z. Ai, M. Huang, D. Shi, Y. Shao, X. Hao, B. Zhang, Y. Wu, Type II cuprous oxide/graphitic carbon nitride p-n heterojunctions for enhanced photocatalytic nitrogen fixation, J. Catal. 395 (2021) 273–281.

[40] D. Zhang, B. Wang, X. Gong, Z. Yang, Y. Liu, Selective reduction of nitrate to nitrogen gas by novel Cu_2O-Cu^0@Fe^0 composite combined with HCOOH under UV radiation, Chem. Eng. J. 359 (2019) 1195–1204.

[41] R. Su, S. Ge, H. Li, Y. Su, Q. Li, W. Zhou, B. Gao, Q. Yue, Synchronous synthesis of Cu_2O/Cu/rGO@carbon nanomaterials photocatalysts via the sodium alginate hydrogel template method for visible light photocatalytic degradation, Sci. Total Environ. 693 (2019), 133657.

[42] D.D. Zhang, M. Halidan, A. Abuduheiremu, Y. Gunisakezi, F.C. Sun, M. Wei, Synthesis and photocatalytic CO_2 reduction performance of Cu_2O/Coal-based carbon nanoparticle composites, Chem. Phys. Lett. 700 (2018) 27–35.

[43] K. Li, C. Sun, Z.Q. Chen, H.X. Qu, H.F. Xie, Q. Zhong, Fe-carbon dots enhance the photocatalytic nitrogen fixation activity of TiO_2@CN heterojunction, Chem. Eng. J. 429 (2022), 132440.

[44] M.J. Cai, C.C. Wang, Y.P. Liu, R.Y. Yan, S.J. Li, Boosted photocatalytic antibiotic degradation performance of $Cd_{0.5}Zn_{0.5}S$/carbon dots/Bi_2WO_6 S-scheme heterojunction with carbon dots as the electron bridge, Sep. Purif. 300 (2022), 121892.

[45] Z.A. Shaikh, N. Moiseev, A. Mikhaylov, S. Yüksel, Facile synthesis of copper oxide-cobalt oxide/nitrogen-doped carbon (Cu_2O-Co_3O_4/CN) composite for efficient water splitting, Appl. Sci. 11 (2021) 9974.

[46] A. Verma, S. Kumar, W.K. Chang, Y.P. Fu, Bi-functional Ag-Cu_xO/g-C_3N_4 hybrid catalysts for the reduction of 4-nitrophenol and the electrochemical detection of dopamine, Dalton Trans. 49 (2020) 625–663.

[47] Y. Hou, N. Deng, F. Han, X. Kuang, X. Zheng, Highly efficient urea-anodizing to promote the electrochemical nitrogen reduction process, Catal. Sci. Technol. 10 (2020) 7819–7823.

[48] H.D. Ji, P.H. Du, D.Y. Zhao, S. Li, F.B. Sun, E.C. Duin, Liu Wen, 2D/1D graphitic carbon nitride/titanate nanotubes heterostructure for efficient photocatalysis of sulfamethazine under solar light: catalytic "hot spots" at the rutile–anatase–titanate interfaces, Appl. Catal., B 263 (2020), 118357.

[49] Y. Liu, L. Chen, X. Liu, T. W. Q, M. Yao, W. Liu, H.D. Ji, Tuning band structure of graphitic carbon nitride for efficient degradation of sulfamethazine: atmospheric condition and theoretical calculation, Chin. Chem. Lett. 33 (2022) 1385–1389.

[50] S. Yanagida, T. Yajima, T. Takei, N. Kumada, Removal of hexavalent chromium from water by Z-scheme photocatalysis using TiO_2 (rutile) nanorods loaded with Au core-Cu_2O shell particles, J. Environ. Sci. (China) 115 (2022) 173–189.

[51] Z.H. Xu, S.J. Ye, G.L. Zhang, W.B. Li, C.J. Gao, C. Shen, Q. Meng, Antimicrobial polysulfone blended ultrafiltration membranes prepared with Ag/Cu_2O hybrid nanowires, J. Membr. Sci. 509 (2016) 83–93.

[52] H. Piao, G. Choi, X. Jin, S.J. Hwang, Y.J. Song, S.P. Cho, J.H. Choy, Monolayer graphitic carbon nitride as metal-free catalyst with enhanced performance in photo- and electro-catalysis, Nano-Micro Lett. 14 (2022) 55.

[53] T. Bhowmick, A. Ghosh, S. Nag, S.B. Majumder, Sensitive and selective CO_2 gas sensor based on CuO/ZnO bilayer thin-film architecture, J. Alloys Compd. 903 (2022), 163871.

[54] L. Huang, F. Peng, H. Yu, H. Wang, Preparation of cuprous oxides with different sizes and their behaviors of adsorption, visible-light driven photocatalysis and photocorrosion, Solid State Sci. 11 (2009) 129–138.

[55] Z. Ren, F. Chen, K. Wen, J. Lu, Enhanced photocatalytic activity for tetracyclines degradation with Ag modified g-C_3N_4 composite under visible light, J. Photochem. Photobiol., A 389 (2020), 112217.

[56] H. Wang, J. Zhang, X. Yuan, L. Jiang, Q. Xia, H. Chen, Photocatalytic removal of antibiotics from natural water matrices and swine wastewater via Cu(I)

coordinately polymeric carbon nitride framework, Chem. Eng. J. 392 (2020), 123638.
[57] X. Xu, L. Meng, Y. Dai, M. Zhang, C. Sun, S. Yang, H. He, S. Wang, H. Li, Bi spheres SPR-coupled Cu_2O/Bi_2MoO_6 with hollow spheres forming Z-scheme Cu_2O/Bi_2MoO_6 heterostructure for simultaneous photocatalytic decontamination of sulfadiazine and Ni(II), J. Hazard Mater. 381 (2020), 120953.
[58] F. Guo, X. Huang, Z. Chen, H. Sun, L. Chen, Prominent co-catalytic effect of CoP nanoparticles anchored on high-crystalline g-C_3N_4 nanosheets for enhanced visible-light photocatalytic degradation of tetracycline in wastewater, Chem. Eng. J. 395 (2020), 125118.
[59] Y.P. Zhu, M. Li, Y.L. Liu, T.Z. Ren, Z.Y. Yuan, Carbon-doped ZnO hybridized homogeneously with graphitic carbon nitride nanocomposites for photocatalysis, J. Phys. Chem. C 118 (2014) 10963–10971.
[60] J. Liu, X. Li, L. Dai, Water-assisted growth of aligned carbon nanotube–ZnO heterojunction arrays, Adv. Mater. 18 (2006) 1740–1744.
[61] W. Zhou, L. Fu, L. Zhao, X. Xu, W. Li, M. Wen, Q. Wu, Novel core-sheath Cu/Cu_2O-ZnO-Fe_3O_4 nanocomposites with high-efficiency chlorine-resistant bacteria sterilization and trichloroacetic acid degradation performance, ACS Appl. Mater. Interfaces 13 (2021) 10878–10890.
[62] H. Li, Y. Qiang, W. Zhao, S. Zhang, 2-Mercaptobenzimidazole-inbuilt metal-organic-frameworks modified graphene oxide towards intelligent and excellent anti-corrosion coating, Corrosion Sci. 191 (2021), 109715.
[63] S. Dong, L. Cui, W. Zhang, L. Xia, S. Zhou, C.K. Russell, M. Fan, J. Feng, J. Sun, Double-shelled $ZnSnO_3$ hollow cubes for efficient photocatalytic degradation of antibiotic wastewater, Chem. Eng. J. 384 (2020), 123279.
[64] T. Wang, Q. Men, X. Liu, H. Zhan, Y. Wang, A staggered type of 0D/2D $CuInS_2$/NiAl-LDH heterojunction with enhanced photocatalytic performance for the degradation of 2,4-Dichlorophenol, Separ. Purif. Technol. 294 (2022), 121215.
[65] W. Liu, M. Wang, C. Xu, S. Chen, Facile synthesis of g-C_3N_4/ZnO composite with enhanced visible light photooxidation and photoreduction properties, Chem. Eng. J. 209 (2012) 386–393.
[66] S. Vignesh, G. Palanisamy, M. Srinivasan, N. Elavarasan, K. Bhuvaneswari, G. Venkatesh, T. Pazhanivel, P. Ramasamy, M.A. Manthrammel, M. Shkir, Fabricating SnO_2 and Cu_2O anchored on g-C_3N_4 nanocomposites for superior photocatalytic various organic pollutants degradation under simulated sunlight exposure, Diam. Relat. Mater. 120 (2021), 108606.
[67] Y. Li, H. Huo, W. Chen, H. Li, L. Gao, S. Yi, Efficient photocatalytic degradation of tetracycline under visible light by AgCl/$Bi_{12}O_{15}Cl_6$/g-C_3N_4 with a dual electron transfer mechanism, Colloids Surf. A Physicochem. Eng. Asp. 638 (2022), 128227.
[68] C.C. Wang, R.Y. Yan, M.J. Cai, Y.P. Liu, S.J. Li, A novel organic/inorganic S-scheme heterostructure of TCPP/$Bi_{12}O_{17}Cl_2$ for boosting photodegradation of tetracycline hydrochloride: kinetic, degradation mechanism, and toxic assessment, Appl. Surf. Sci. 610 (2022), 155346.
[69] Z. Li, L. Schulz, C. Ackley, N. Fenske, Adsorption of tetracycline on kaolinite with pH-dependent surface charges, J. Colloid Interface Sci. 351 (2010) 254–260.
[70] Y. Yang, C. Zhang, C. Lai, G. Zeng, D. Huang, M. Cheng, J. Wang, F. Chen, C. Zhou, W. Xiong, BiOX (X=Cl, Br, I) photocatalytic nanomaterials: applications for fuels and environmental management, Adv. Colloid Interface Sci. 254 (2018) 76–93.
[71] H. Guo, H.Y. Niu, C. Liang, C.G. Niu, Y. Liu, N. Tang, Y. Yang, H.Y. Liu, Y.Y. Yang, W.J. Wang, Few-layer graphitic carbon nitride nanosheet with controllable functionalization as an effective metal-free activator for peroxymonosulfate photocatalytic activation: role of the energy band bending, Chem. Eng. J. 401 (2020), 126072.
[72] L. Wang, X. Ma, G. Huang, R. Lian, J. Huang, H. She, Q. Wang, Construction of ternary CuO/$CuFe_2O_4$/g-C_3N_4 composite and its enhanced photocatalytic degradation of tetracycline hydrochloride with persulfate under simulated sunlight, J. Environ. Sci. (China) 112 (2022) 59–70.
[73] J.B. Wang, D. Zhi, H. Zhou, X.W. He, D.Y. Zhang, Evaluating tetracycline degradation pathway and intermediate toxicity during the electrochemical oxidation over a Ti/Ti_4O_7 anode, Water Res. 137 (2018) 324–334.
[74] L.J. Wang, Z. Zhang, R.Q. Guan, D.D. Wu, W.L. Shi, L.M. Yu, P. Li, W. Wei, Z. Zhao, Z.C. Sun, Synergistic CO_2 reduction and tetracycline degradation by CuInZnS-$Ti_3C_2T_x$ in one photoredox cycle, Nano Res. 15 (2022) 8010–8018.
[75] J.D. Li, F. Wei, Z.Y. Xiu, X.J. Han, Direct Z-scheme charge transfer of Bi_2WO_6/$InVO_4$ interface for efficient photocatalytic CO_2 reduction, Chem. Eng. J. 446 (2022), 137129.
[76] C.C. Ma, S.T.U. Din, W.C. Seo, J. Lee, Y. Kim, H. Jung, W. Yang, $BiVO_4$ ternary photocatalyst co-modified with N-doped graphene nanodots and Ag nanoparticles for improved photocatalytic oxidation: a significant enhancement in photoinduced carrier separation and broad-spectrum light absorption, Separ. Purif. Technol. 264 (2021), 118423.
[77] W.L. Shi, C. Liu, M.Y. Li, X. Lin, F. Guo, J.Y. Shi, Fabrication of ternary Ag_3PO_4/$Co_3(PO_4)_2$/g-C_3N_4 heterostructure with following Type II and Z-Scheme dual pathways for enhanced visible-light photocatalytic activity, J. Hazard Mater. 389 (2020), 121907.
[78] P. Xiao, D.L. Jiang, L.X. Ju, J.J. Jing, M. Chen, Construction of RGO/$CdIn_2S_4$/g-C_3N_4 ternary hybrid with enhanced photocatalytic activity for the degradation of tetracycline hydrochloride, Appl. Surf. Sci. 433 (2018) 388–397.
[79] Q. Liang, S. Cui, J. Jin, C.H. Liu, S. Xu, C. Yao, Z.Y. Li, Fabrication of BiOI@UIO-66(NH_2)@g-C_3N_4 ternary Z-scheme heterojunction with enhanced visible-light photocatalytic activity, Appl. Surf. Sci. 456 (2018) 899–907.
[80] H. Ramezanalizadeh, E. Rafiee, Very fast photodegradation of tetracycline by a novel ternary nanocomposite as a visible light driven photocatalyst, Mater. Chem. Phys. 261 (2021), 124242.
[81] F. Chen, Q. Yang, Y.L. Wang, J.W. Zhao, D.B. Wang, X.M. Li, Z. Guo, H. Wang, Y.C. Deng, C.G. Niu, G.M. Zeng, Novel ternary heterojunction photco-catalyst of Ag nanoparticles and g-C_3N_4 nanosheets co-modified $BiVO_4$ for wider spectrum visible-light photocatalytic degradation of refractory pollutant, Appl. Catal., B 205 (2017) 133–147.
[82] F. Guo, X.L. Huang, Z.H. Chen, L.W. Cao, X.F. Cheng, L.Z. Chen, W.L. Shi, Construction of Cu_3P-$ZnSnO_3$-g-C_3N_4 p-n-n heterojunction with multiple built-in electric fields for effectively boosting visible-light photocatalytic degradation of broad-spectrum antibiotics, Separ. Purif. Technol. 265 (2021), 118477.
[83] X.D. Jiang, S.F. Lai, W.C. Xu, J.Z. Fang, X. Chen, J.Z. Beiyuan, X.W. Zhou, K.C. Lin, J.X. Liu, G.C. Guan, Novel ternary BiOI/g-C_3N_4/CeO_2 catalysts for enhanced photocatalytic degradation of tetracycline under visible-light radiation via double charge transfer process, J. Alloys Compd. 809 (2019), 151804.
[84] W. Zhao, Y.J. Li, P.S. Zhao, L.L. Zhang, B.L. Dai, J.M. Xu, H.B. Huang, Y.L. He, D.Y.C. Leung, Novel Z-scheme Ag-C_3N_4/SnS_2 plasmonic heterojunction photocatalyst for degradation of tetracycline and H_2 production, Chem. Eng. J. 405 (2021), 126555.